Hindawi
International Journal of Antennas and Propagation
Volume 2018, Article ID 6759394, 10 pages
https://doi.org/10.1155/2018/6759394

Research Article

Analysis of Static Narrowband On-Body Channel Polarization Distribution at 2.4 GHz

Lingfeng Liu, Peng Zhang, Xiaonan Wang, Xiaoyan Zhang, and Nan Jiang

School of Information Engineering, East China Jiaotong University, Nanchang, China

Correspondence should be addressed to Lingfeng Liu; lingfeng.liu@163.com and Peng Zhang; 15965741178@163.com

Received 22 June 2018; Revised 20 August 2018; Accepted 30 August 2018; Published 3 October 2018

Academic Editor: Ana Alejos

The polarization of on-body propagation channels has shown significant spatial selectivity and full-space distribution in numerous measurements due to the near-field characteristics and strong body scattering effect. To get a comprehensive image of such polarization distribution, in this work, we measured polarized on-body channels on static body at 2.4 GHz by monopole antennas, where standing and sitting postures are included. The polarization of the measured on-body antennas covers the full-space in *Z*-, *H*-, and *V*-direction relative to the skin of the body. Consequently, an extended cross-polarization discrimination (XPD) is also proposed to describe the depolarization and copolarization in the measurements. In the statistical characteristics of the channels, the *V*-polarization direction of the receiving antenna is more conducive for receiving signal and reducing the path losses. The results show that strong depolarization of on-body channels is more easily caused in sitting posture due to scattering effects from the legs. Simplified finite-difference-time-domain (FDTD) simulations are conducted to investigate the field polarization distribution of point sources on a static torso in cylindrical shape. The simulation results are in general consistent with the analysis of measured on-body channels.

1. Introduction

On-body communications in wireless body area networks (WBANs) are short distance communications (<2 m) [1] defined on or above the body of limited height. This type of propagation channels occurs under great chance in near-field range and is heavily coupled by the body [2–4], i.e., the propagation environment and the antennas. Conventional far-field propagation theories may not fully describe the complex distribution of on-body channels in the form of surface wave [5, 6] and may fail to optimize the communication by missing the propagation components. Studies as [7, 8] have shown the high sensitivity of on-body channels to the orientation of the transmission and receiving antennas, implying the effectiveness of polarization diversity with a wearable BAN.

Earlier study on the finite-difference-time-domain (FDTD) simulations of the electromagnetic fields on the body surface has shown that due to the near-field body scattering effects, the surface wave propagation assumption may not fully consistent with the actual wave propagation in on-body channels, resulting the channel polarization dispersion both along and normal to the propagation path defined. The postures and body dynamics will further lead to the variation of the on-body polarization distribution over time and space domains. One limitation of previous measurements as reported in [9–11] is that most of the measurements cover partial polarization combinations of on-body channels. Consequently, the polarization matrix of the channels is not fully characterized and modeled. Full-space description of the channel polarization distribution under specific scenarios is necessary to correctly capture the field components of the on-body channels.

In this work, measurements of polarized narrowband on-body channels at 2.4 GHz on static human body are conducted in indoor environment. Full polarization combinations are investigated for channels covering the key parts of the body. Two static postures of the body, i.e., the standing and sitting postures, were investigated, and the channel polarization distributions under the two postures were compared. The polarization matrix and the cross-polarization discrimination (XPD) for each scenario

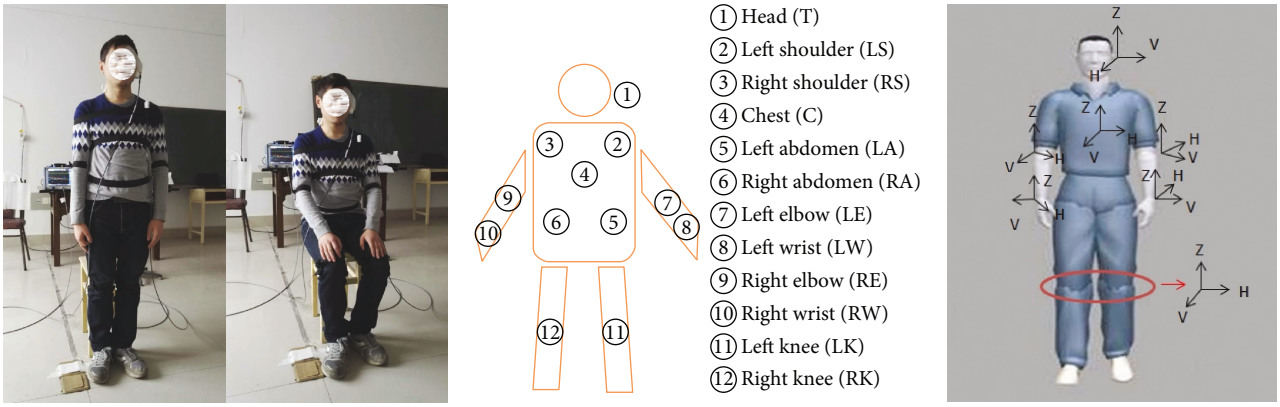

(a) (b) (c)

Figure 1: Measurement context at 2.4 GHz. (a) Indoor scenario and human body postures. (b) Node placement on the body. (c) The definition of polarization direction in different parts of the body.

are summarized. Numerical simulations such as finite-difference-time-domain (FDTD) methods are capable to provide a full description of the field polarization distribution on the bodies [12]. Here, FDTD simulations are conducted to study the field polarization distribution of point sources placed on a static torso. Simplified body modelling numerical simulations may help to explain the physical mechanisms of on-body channel polarization distribution.

This paper is organized as follows. Section 2 describes the configuration of the measurements. Section 3 introduces the statistical analysis of the channel polarization distribution and depolarization characteristics. Section 4 presents the comparative analysis by FDTD simulations. Finally, Section 5 summarizes the analysis.

2. Measurement Setting

The measurements were carried out in an indoor environment, i.e., an empty laboratory of dimension 6 by 7 meters without large objects around. The primary parts of the measurements were conducted on the torso, hence to limit the ground reflection effect. We thereby assume the environment as reflection negligible, and on-body channels are primarily determined by their geometry distribution and body scattering.

A male volunteer of height 160 cm and weight 50 kg was chosen. Two postures, standing and sitting with arms naturally posed, are investigated as shown in Figure 1(a). The positions of the antennas on the body define the channels as presented in Figure 1(b). The measured channels are listed in Table 1. Narrowband on-body channels at 2.4 GHz frequency band over time domain were measured on the body. To avoid heavy interference from the Wi-Fi signals, the actual frequency was selected at 2.484 GHz, i.e., an extra Wi-Fi channel not used in the China region.

A vector network analyzer (VNA) of type R&S ZNB 20 was applied to measure the channel S-parameters over time domain. The environment was quiet with no significant fading effects observed from the measurement. The analysis is then focused on the average channel loss. Monopole antennas of size 5 cm were used and mounted on the body 2 cm above the skin to alleviate the body coupling effects to the antenna efficiency. Setting details of the VNA and the antenna are presented in Table 2.

Table 1: Measurement sets.

Set number	Channels	Channel abbreviation
1	Head-left shoulder	T-LS
2	Head-left wrist	T-LW
3	Chest-left abdomen	C-LA
4	Left shoulder-chest	LS-C
5	Left elbow-left wrist	LE-LW
6	Head-chest	T-C
7	Head-left abdomen	T-LA
8	Head-left elbow	T-LE
9	Left shoulder-left elbow	LS-LE
10	Left shoulder-right shoulder	LS-RS
11	Left abdomen-right abdomen	LA-RA
12	Left abdomen-left knee	LA-LK
13	Left knee-right knee	LK-RK
14	Left elbow-right elbow	LE-RE
15	Left wrist-right wrist	LW-RW

The field around the human body does not fully follow far-field propagation principles. The propagation path, as commonly defined by the surface wave presumption for on-body channels, may not be strictly perpendicular to the direction of the field polarization due to the body scattering effect and the near-field features of the radio waves. Consequently, this will cause the polarization dispersion onto all directions. To effectively describe such inconsistency between the channel polarization and the propagation path, we propose an extended definition of on-body antenna polarization in full-space dimension relative to the skin, which are vertical tangential (denoted as Z-direction), horizontal tangential (denoted as H-direction), and horizontal normal (denoted as V-direction), as described in Figure 1(c). Note that because of the irregularity of the

Table 2: Radio settings.

Parameter	Value
VNA	ROHDE SCHWAR ZNB 20
Sampling points	1000
Transmit power	10 dBm
IF bandwidth	10 kHz
Sweep time	10 s
Antenna model	Monopole
Antenna size	5 cm

shapes of different parts of the body, the directions may be defined in different global orientations as well. Thereby, an on-body channel's polarization can be decomposed into 9 combinations, denoted as XY, X, and $Y \in \{Z, V, H\}$ expressed in the form of 3 by 3 polarization matrix in (1), where X and Y are the relative orientations, i.e., the polarization of the transmitter and receiver, respectively:

$$\begin{bmatrix} ZZ & VZ & HZ \\ ZV & VV & HV \\ ZH & VH & HH \end{bmatrix}. \quad (1)$$

3. Measurement Statistical Analysis

In general, as the measurements were collected on static body in different postures. The measured channels exhibited close-to-flat channel loss distribution along the time domain. In Table 3, we summarize the average standard deviation (σ) of each channel polarization component in different distribution under two postures. It shows that the fading effect can be ignored in the measurements. Furthermore, Figure 2 shows the PDF of the normalized channel loss, which fit the Gaussian distribution universally for different polarization components. All these show that the measured on-body channels did not suffer from the fading effect and are considered as flat over time in each scenario. Therefore, our analysis focus on the average path losses of on-body channels in different polarization combinations, which are summarized in Table 4 and categorized by the postures, respectively.

3.1. V-Polarization Convergence. The first observation of the channel loss in both postures is that most channels show V-polarization convergence at the receiving side. Under standing posture for instance, the minimal channel losses of scenarios T-LS, C-LA, LS-LE, LS-RS, LA-RA, LK-RK, and LW-RW are achieved in VV channel polarization and ZV channel polarization for T-LW, LS-C, LE-LW, T-C, T-LA, T-LE, and LA-LK scenarios, and only scenario LE-RE is in VZ channel polarization. Similar properties are also observed in these scenarios under the sitting posture. The difference under sitting postures is the LE-LW and LE-RE scenarios. The minimal channel loss of scenario LE-LW is achieved in HH channel polarization, and the minimal channel loss of scenario LE-RE is achieved in VZ channel polarization, a possible consequence of the body coupling effect variation to the antennas during posture changes.

On the contrary, in all scenarios investigated in two postures, the maximal channel loss rarely occurs in channel polarizations with V-polarization at the receiving side for all polarizations at the transmit side. Only scenarios LK-RK and LE-RE under standing posture, the maximal channel loss is observed in channel polarization with V-polarization at the receiving side. As shown in Figure 3, the percentage of V-polarization of the receiving side is up to 90 percent in minimal loss channel polarizations, and Z-polarization at the receiving side should be avoided due to the proportion of up to 57 percent in maximal loss channel polarizations. This indicates that having the receiving antenna in V-polarization helps to capture the majority of the on-body channel field components.

The above observations show that on-body channels tend to have their field distributed along directions normal to the body. The body coupling effect causes the absorbing of the on-body fields tangential to the skin, while the fields normal to the skin are less affected. As a result, the field will make the majority part along the normal direction. This may suggest an optimal antenna emplacement for the communication aspects.

3.2. Channel Depolarization. The results presented in Table 4 show as well heavy cross-polarization in different scenarios. If the on-body communication systems are designed following regular antenna emplacement, i.e., the orientation of the antennas are either in Z-, H-, or V-directions, such cross-polarization may cause the actual field polarization of the on-body channel be apart from these regular directions. We denote this as the channel depolarization effect.

There are three depolarization scenarios which can be studied with the available data. There are two subscenarios in each scenario. They include change of the Z-polarization into the V- or H-direction component at the receiving antenna. This effect can be characterized by comparing ZZ with ZV or ZH configurations (scenarios ZZ-ZV and ZZ-ZH). Depolarization from the V into Z- or H-polarization is characterized by comparing VV with VZ or VH configurations (scenarios VV-VZ and VV-VH). Similarly, the depolarization from the H into Z- or V-polarization at the receiving antenna is characterized (scenarios HH-HZ and HH-HV). The cross-polarization discrimination (XPD) for these three cases is defined as follows:

$$\text{XPD} = \frac{P_{ii}}{P_{ij}}, \quad (2)$$

where $i, j \in \{V, H, Z\}$, $i \neq j$, P_{ii} is the power of the copolarized channel component, and P_{ij} is the cross-polarized channel component.

Figures 4–6 show the XPD values for three scenarios in two postures. If XPDs of both subscenarios are positive, which indicates that the copolarization remains dominant in these channels, the higher of the value indicates that the channel tends to concentrate on its copolarization

Table 3: The average standard deviation (σ) of on-body channel path gain during measurement times in 9 polarizations. The value 0 represents $\sigma < 0.1$.

Channel	T-LS	T-LW	C-LA	LS-C	LE-LW	T-C	T-LA	T-LE	LS-LE	LS-RS	LA-RA	LA-LK	LK-RK	LE-RE	LW-RW
Stand (σ)	0.2	0.4	0.6	0.7	0.4	0.2	0.2	0.5	0.6	1.1	0.7	0.3	0.1	0.5	0.9
Sit (σ)	0	0.1	0.2	0.4	0.2	0.5	0.1	0.1	0.3	0.4	0.3	0.4	0.1	0.2	0.1

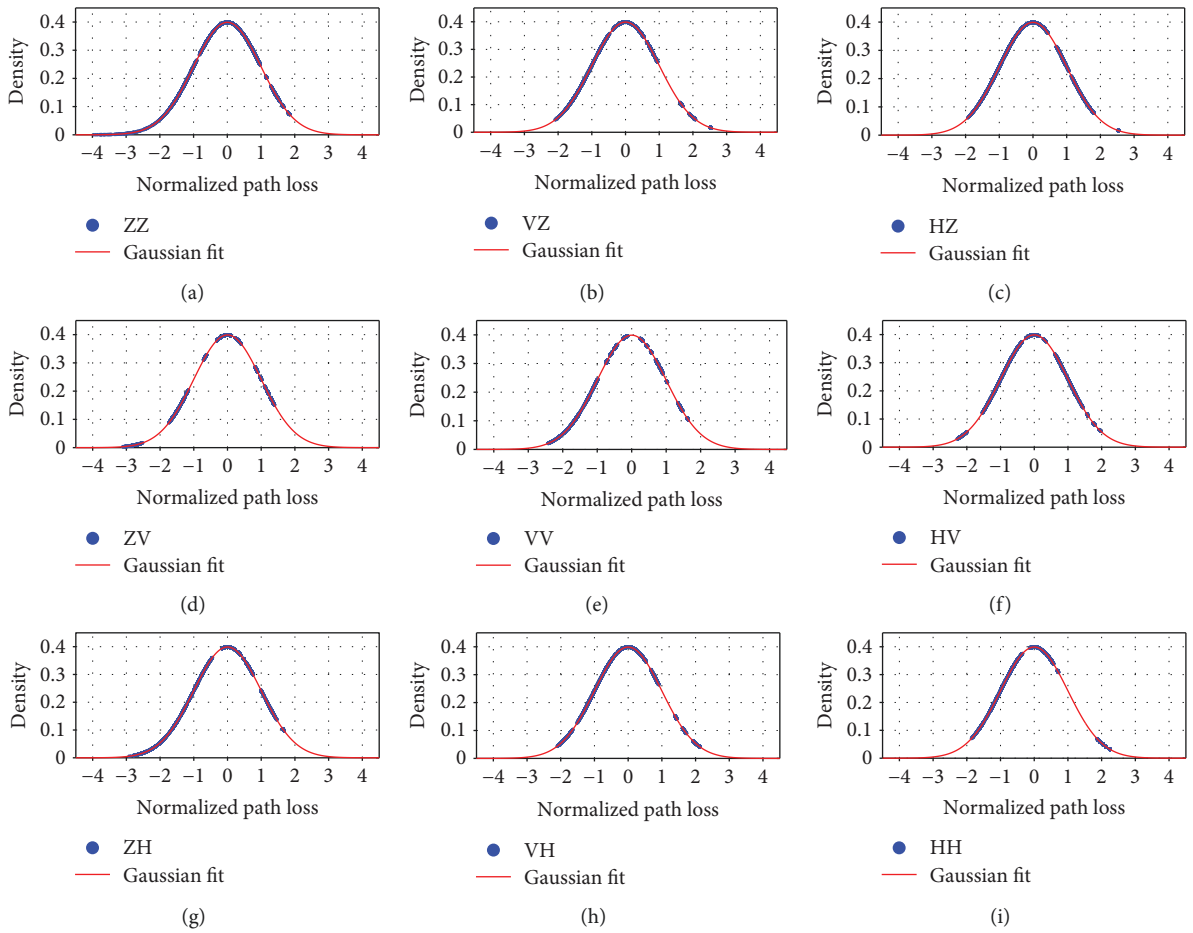

Figure 2: PDF of normalized channel loss of on-body channels for measurements in 9 polarizations and Gaussian fit (red line) for 9 polarizations: (a) *ZZ*, (b) *VZ*, (c) *HZ*, (d) *ZV*, (e) *VV*, (f) *HV*, (g) *ZH*, (h) *VH*, and (i) *HH*.

component. If the XPD of a subscenario is negative, and the other is positive or close to 0 dB, we think that the cross-polarized configurations remain dominant in on-body channels, the smaller of the negative value indicates that the channel is transmitting its fields to the cross-polarization component. Similarly, both subscenarios are negative and the values are not approximately equal, and we also think that the cross-polarization remains dominant in these links. There are three situations here that indicate a strong depolarization in the channel. The first is that the XPD values of both subscenarios are close to 0 dB, and the field will be projected both onto the copolarized and cross-polarized components of the channel. Similarly, a subscenario is positive and the other is close to 0 dB. Finally, XPDs of two subscenarios are negative and approximately equal, and the field will be projected both onto two cross-polarized components of the channel.

Figures 4(a) and 4(b) show the XPD of on-body channels with the transmitting antenna-adopted *Z*-polarization in the two postures. We can find that the cross-polarization remains dominant in most on-body channels, where the XPD values of both subscenarios are negative in these links. The receiving antenna can generally obtain the main component of the field in the *V*-polarization direction by comparing subscenarios *ZZ-ZV* with *ZZ-ZH*, regardless of the standing or sitting postures. When the transmission antenna adopts *Z*-polarization, *ZV* channel polarization is better suited to most of on-body channels than *ZH* channel polarization because of the larger absolute XPD. As shown in Figure 4(a), unlike the other cross-polarized on-body

Table 4: Path loss summary of measurements (dB).

Standing/sitting	*ZZ*	*ZV*	*ZH*	*VZ*	*VV*	*VH*	*HZ*	*HV*	*HH*
T-LS	37.18/35.58	25.39/26.75	27.18/27.69	29.74/23.83	23.60/23.65	28.83/34.50	41.04/29.66	28.98/27.75	26.72/24.80
T-LW	58.11/53.47	37.21/39.17	47.79/39.60	59.12/58.62	42.78/47.17	61.49/46.49	61.84/58.22	48.39/39.24	62.10/43.51
C-LA	65.36/43.84	36.70/40.94	48.95/50.46	49.86/46.75	29.90/25.34	39.78/38.79	63.44/38.53	36.34/33.60	54.88/41.84
LS-C	50.38/47.02	30.32/30.60	43.70/48.15	49.68/50.81	30.69/31.09	54.65/50.89	54.81/45.27	35.68/36.66	45.71/46.30
LE-LW	47.66/39.05	23.92/35.77	31.12/32.07	42.14/44.11	29.99/28.52	29.93/32.32	50.10/56.16	30.33/33.52	27.97/25.91
T-C	45.97/45.10	27.51/27.41	35.55/38.78	53.95/52.90	33.26/32.26	39.01/43.07	52.22/57.00	32.86/35.46	42.53/46.57
T-LA	53.96/45.74	29.17/28.77	43.78/40.21	63.14/45.68	38.61/38.26	55.20/51.24	64.89/49.31	41.26/41.04	58.91/44.02
T-LE	52.52/58.57	39.76/40.06	40.47/42.15	61.44/41.09	49.88/50.31	53.16/52.09	59.55/50.65	44.75/42.28	45.49/52.21
LS-LE	49.87/56.85	36.44/35.63	46.46/45.42	66.39/52.59	34.45/34.64	44.46/48.12	65.57/55.97	49.97/42.88	52.49/52.21
LS-RS	65.00/63.36	47.86/42.85	56.40/55.07	50.49/57.40	31.03/33.33	43.52/41.78	44.27/41.47	51.04/40.80	57.94/50.32
LA-RA	67.17/54.91	55.91/42.75	77.42/64.52	51.52/47.64	38.11/41.73	44.31/45.01	59.26/60.85	47.67/46.22	56.08/52.24
LA-LK	55.29/66.15	39.52/40.96	46.29/59.52	68.03/59.26	40.67/53.56	50.39/57.13	58.28/50.79	45.47/45.81	51.26/53.83
LK-RK	38.79/41.67	53.56/43.49	44.17/46.81	42.85/43.27	30.40/34.39	42.26/46.57	49.20/44.36	45.26/44.45	46.22/51.43
LE-RE	66.23/59.43	68.93/58.08	60.67/66.84	33.22/63.41	45.89/51.19	49.52/47.38	36.53/59.71	41.45/49.75	39.80/59.75
LW-RW	58.34/48.28	55.36/57.27	73.49/58.95	69.84/51.33	40.65/36.24	60.09/46.14	61.71/59.52	56.70/48.95	57.15/52.88

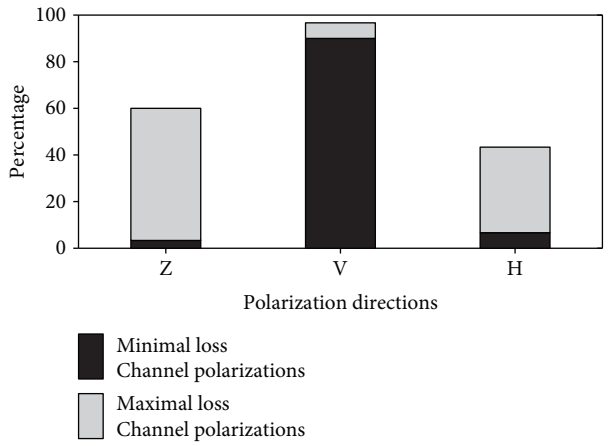

Figure 3: The percentage of 3 polarizations of the receiving side in minimal loss channel polarizations and maximal loss channel polarizations, respectively.

channels in the standing posture, the copolarization takes the dominant component in the channel LK-RK and the channel LW-RW is strongly depolarized due to the XPD of the subscenario *ZZ-ZH* is close to 0 dB and the other is positive. In the sitting posture, the polarization of channel LW-RW is stronger than that of the standing-state and the copolarization occupies the dominant component because of positive XPD of both subscenarios, and the channel LK-RK becomes strongly depolarized as shown in Figure 4(b). The strong depolarization also occurred in channels C-LA and LE-RE in sitting posture. These indicate that the effect of posture on polarization characteristics of on-body channels is different for different channels.

When the transmitting antenna of the on-body channel adopts *V*-polarization in the two postures, the XPDs of on-body channels are shown in Figures 5(a) and 5(b). Positive XPDs of both subscenarios for most on-body channels confirm that the antennas remain mostly copolarized in these links. Under the standing posture, unlike the other copolarized on-body channels, channels LE-LW and T-LE are strongly depolarized due to the XPD of subscenario *VV-VZ* which is positive and the other is close to 0 dB as shown in Figure 5(a). The cross-polarization remains dominant only in channel LE-RE, with negative XPD of subscenario *VV-VZ* and XPD of subscenario *VV-VH* closes to 0 dB. Figure 5(b) shows that the polarization of channel LE-RE is weakened in the sitting posture and even strong depolarization occurred in the channel. The strong depolarization also occurred in other channels, such as T-LS, T-LW, and LE-LW channels. These show that human sitting posture is more likely to cause depolarization of on-body channels with the transmitting antenna-adopted *V*-polarization.

As shown in Figures 6(a) and 6(b), subscenarios *HH-HZ* and *HH-HV* show that the polarization characteristics of the channels are different for different on-body channels when the transmitting antenna is *H*-polarized in either standing or sitting posture. As shown in Figure 6(a), under the standing posture, the characteristics of on-body channels appear in two ways: cross-polarization or strong depolarization, for example, strong depolarization channels T-LS, LE-LW, and T-LE; cross-polarized channels T-LW, and C-LA, LS-C. Similarly, there are mainly cross-polarized channels and strong depolarization channels in the sitting posture as shown in Figure 6(b). One exception under sitting postures is the channel LE-LW, where the copolarization remains dominant. From this, it can be found that the receive field components are mainly distributed in the *V*- and *Z*-polarization directions for most on-body propagation channels with transmitting antenna-adopted *H*-polarization, regardless of the standing or sitting postures.

According to the analysis of the above three scenarios, we can find that the receiving antenna can generally obtain the decent component of the field in the *V*-polarization

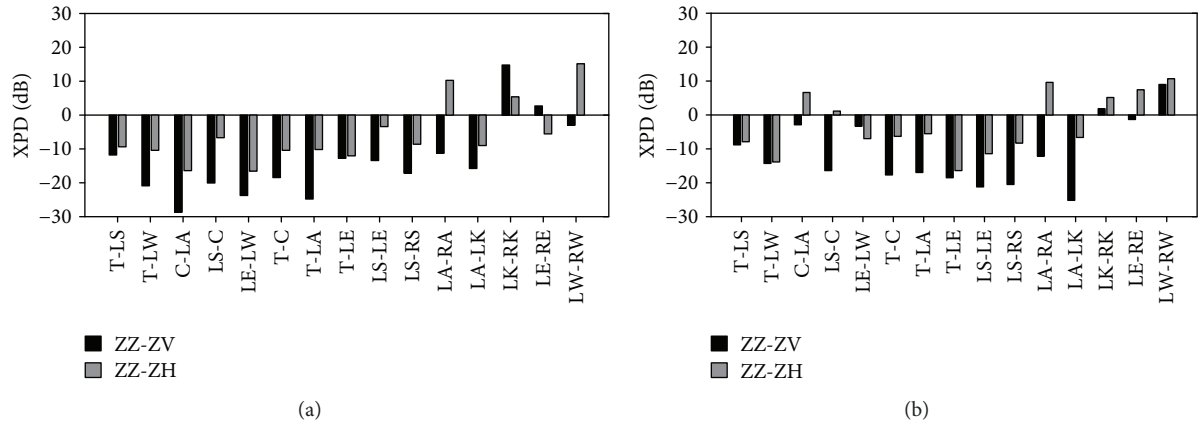

Figure 4: XPD of on-body channels in two postures. (a) XPD of scenarios *ZZ-ZV* and *ZZ-ZH* in the standing posture. (b) XPD of scenarios *ZZ-ZV* and *ZZ-ZH* in the sitting posture.

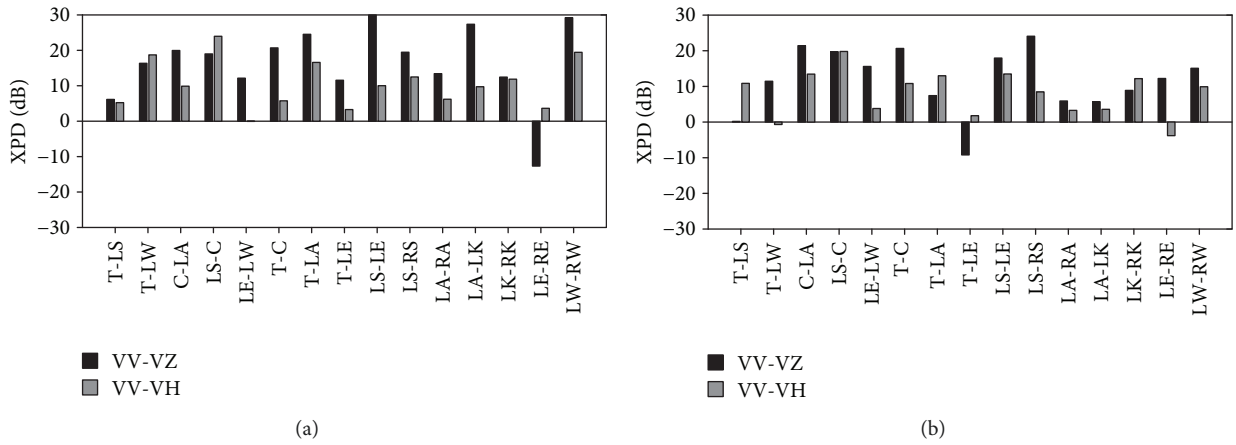

Figure 5: XPD of on-body channels in two postures. (a) XPD of scenarios *VV-VZ* and *VV-VH* in the standing posture. (b) XPD of scenarios *VV-VZ* and *VV-VH* in the sitting posture.

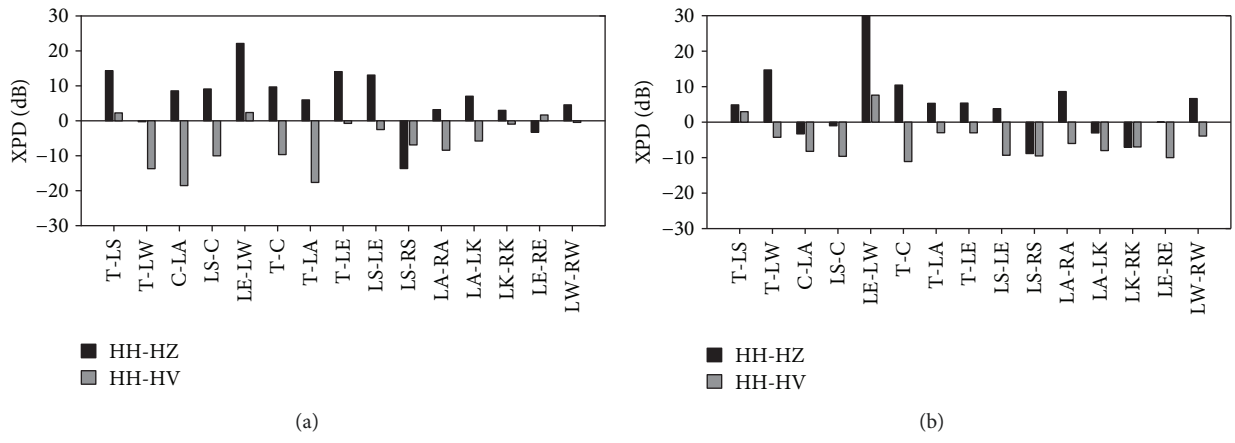

Figure 6: XPD of on-body channels in two postures. (a) XPD of scenarios *HH-HZ* and *HH-HV* in the standing posture. (b) XPD of scenarios *HH-HZ* and *HH-HV* in the sitting posture.

direction, regardless of the polarization direction of the transmission antenna. At the same time, this is also the reason why the receiving antenna with *V*-polarization can effectively receive signal and reduce the path loss.

4. Comparative Analysis by FDTD Simulations

4.1. Geometry Model and Radio Configuration. Simplified FDTD simulations are made to further understand the

channel properties in the simulation. We modeled a human torso by a cylinder of finite length as in Figure 7 to avoid the irregular shape impacts to the simulation. The selected cylinder is of length 1 m and radius 0.25 m. To alleviate the antenna size and structure effects to the on-body EM field distribution, a monopole antenna of length 3 mm is selected to simulate a point current source. The detailed configuration of the simulation is given in Table 5. The FDTD simulation is carried in XFDTD®7.3.0. The narrowband on-body channels at 2.484 GHz are investigated. A 50-ohm current source is applied given current intensity of $1e-10$ A and sinusoid waveforms. The source is fed onto a monopole antenna of length 3 mm. Without considering the antenna efficiency, the dimension of the antenna is negligible compared with the dimension of the cylinder and can approximate a point source in the simulations. The torso is constituted by homogeneous lossy biotissue, i.e., dry skin in this work, based on the observation that radio signals at 2.484 GHz will decay fast when penetrating the body. The dielectric coefficients of the dry skin are derived from the Cole-Cole model [13]. To alleviate the computation load, the mesh grid of the FDTD is limited to 2.5 mm in all the directions.

The polar-z coordinate system is applied by orienting the cylinder along the z-axis. The field distribution is then symmetrical along z. The point current source is placed at location expressed in Cartesian coordinate and polar-z coordinate, respectively, as follows:

$$(x_s, y_s, z_s) = (0, 0.25 + d_{ss}, 0.5),$$
$$(z_s, \rho_s, \phi_s) = \left(0.5, 0.25 + d_{ss}, \frac{\pi}{2}\right), \quad (3)$$

where d_{ss} is the distance from the source to the skin. For on-body wireless sensors, d_{ss} is confined between a maximum value to correspond to sensors attached on the skin and a minimal value to alleviate the body coupling effect to the antennas. In our investigation, the range of d_{ss} is limited between 1 and 5 cm. For simplicity, the following analysis is focused on scenarios with $d_{ss} = 3$ cm as a median reference source-surface distance.

In this simulation, we define three polarization directions of the point source, z, ρ and ϕ, which correspond, respectively, to the polarization directions Z, V, and H defined in (1).

Three dimensions of the on-body field distribution are investigated as in Figure 7:

(1) Horizontal planes dissecting the torso described by δ_z

(2) Circles around the torso described by δ_z and δ_ρ

(3) Radial lines to illustrate the field variation with respect to δ_ρ changes, described by δ_z and δ_ϕ

The electronic fields are computed in the simulations, denoted as E_Y^X, X, and $Y \in \{z, \rho, \phi\}$. The strength of the polarization is then computed as $|E_Y^X|^2$. For simplicity, E_Y^X is used in the following part to denote the on-body channel polarization strength as well. In addition, when the polarization direction of the transmitter has been declared, E_Y^X will be simplified to E_Y.

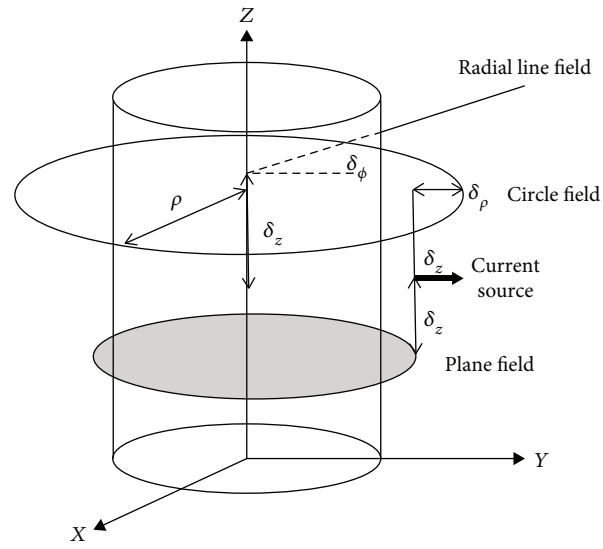

Figure 7: Geometry model of a static torso and plane, circle, and radial line dimension definition on torso.

Table 5: Radio configuration of FDTD simulations.

Current intensity	$1e-10$ A
Frequency (single)	2.484 GHz
Dry skin conductivity	0.597488 S/m
Dry skin relative permittivity	38.0066
FDTD boundary conditions	Absorbing
Mesh size (all conditions)	2.5 mm

4.2. FDTD Result Analysis. The FDTD simulations investigate scenarios of δ_z at 0.4 m due to this distance which corresponds to the length of most measured on-body channels. The study focuses on the circles around the torso and the radial lines normal to the torso as explained in Figure 7.

Figure 8 presents the field polarization distribution on the circle around the torso at $\delta_z = 0.4$ m and $\delta_\rho = 0$, when source in polarization z, ρ, and ϕ, respectively. Here, we mainly analyze the visual range $\delta_\phi \in [0^\circ\ 180^\circ]$ due to in line with the measured on-body propagation channels. Figure 8(a) shows that E_ρ^z maintains quasi-linear decaying on dB scale in the region $\delta_\phi \in [0^\circ\ 180^\circ]$, which shows a stable field polarization distribution around the torso. In Figure 8(a), the strength of E_ρ^z remains dominant in the region $\delta_\phi \in \{[0^\circ\ 54^\circ], [70^\circ\ 108^\circ], [131^\circ\ 180^\circ]\}$, which shows that the cross-polarization generally remains dominant in a wide region. Although the strength difference between E_ρ^z and E_ϕ^z closes to 0 dB in the region $\delta_\phi \in \{[54^\circ\ 70^\circ], [108^\circ\ 131^\circ]\}$, the probability of depolarization is small due to the smaller angular range and the receiving antenna can generally obtain the decent component of the field in the

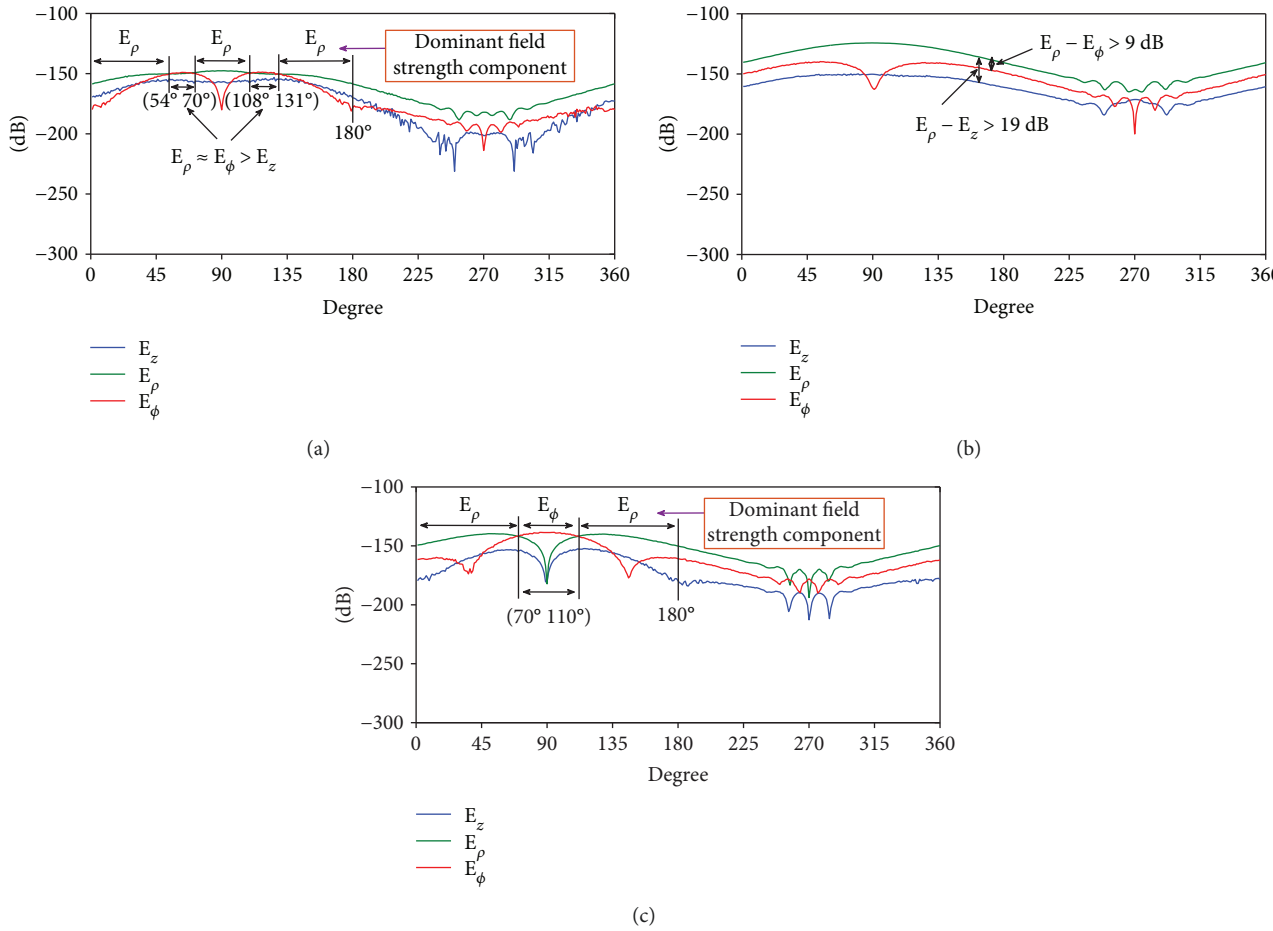

FIGURE 8: Field polarization distribution on horizontal circle $\delta_z = 0.4$ m and $\delta_\rho = 0$. (a) Source in polarization z. (b) Source in polarization ρ. (c) Source in polarization ϕ.

polarization ρ direction in a wide range. The simulation results of source in polarization z are foundationally similar to the analysis for XPD of scenarios *ZZ-ZV* and *ZZ-ZH* in Figure 4.

The fields of source in polarization ρ show quasi-linear decaying distribution at close decaying rates on E_ρ^ρ and E_z^ρ as shown in Figure 8(b), because of the surface wave effect. E_z^ρ is found to be distributed at negligible strength levels compared with the other polarization components. The strength of E_ρ^ρ remains dominant, and the strength difference between E_ρ^ρ and E_ϕ^ρ or E_z^ρ remains higher than 9 dB in the region $\delta_\phi \in [0^\circ\ 180^\circ]$, which indicates that on-body channels have good polarization characteristics and the co-polarization remains dominant in a wide visual region, when the fields of source in polarization ρ. These are similar to actual measurement results of on-body channels with the transmitting antenna-adopted *V*-polarization.

A typical observation of the field distribution of source in polarization ϕ is that the E_ρ^ϕ is generally stronger than E_ϕ^ϕ and E_z^ϕ, which is quite close to the field distribution of source in polarization ρ, as shown in Figure 8(c). This observation may indicate the insensitivity of the field polarization distribution on horizontal planes with respect to the source polarization. These show that the receiving antenna can generally obtain the decent component of the field in the polarization ρ direction when the fields of source in polarization ϕ. Unlike the point source polarization at ρ, the strength of E_ϕ^ϕ remains dominant in the region $\delta_\phi \in [70^\circ\ 110^\circ]$. These simulation results of source in polarization ϕ also show that the polarization characteristics of the channel are obvious and depolarization hardly occurs in on-body channel with the field of source in polarization ϕ, which is different from the XPD analysis of actual measured on-body channels with the transmitting antenna-adopted *H*-polarization as shown in Figure 6. The main reason for this disparity is the complexity of the actual human geometry and the impact of the measurement environment.

Based on the analysis of the simulation results of the above field sources in the three polarization directions, we have found that the receiving antenna generally obtains a decent field component in the polarization ρ, regardless of the source polarization direction. This conclusion is called ρ-polarization convergence. In order to more fully prove the results of this study, a further study should be done. The field distribution along the radial line at location

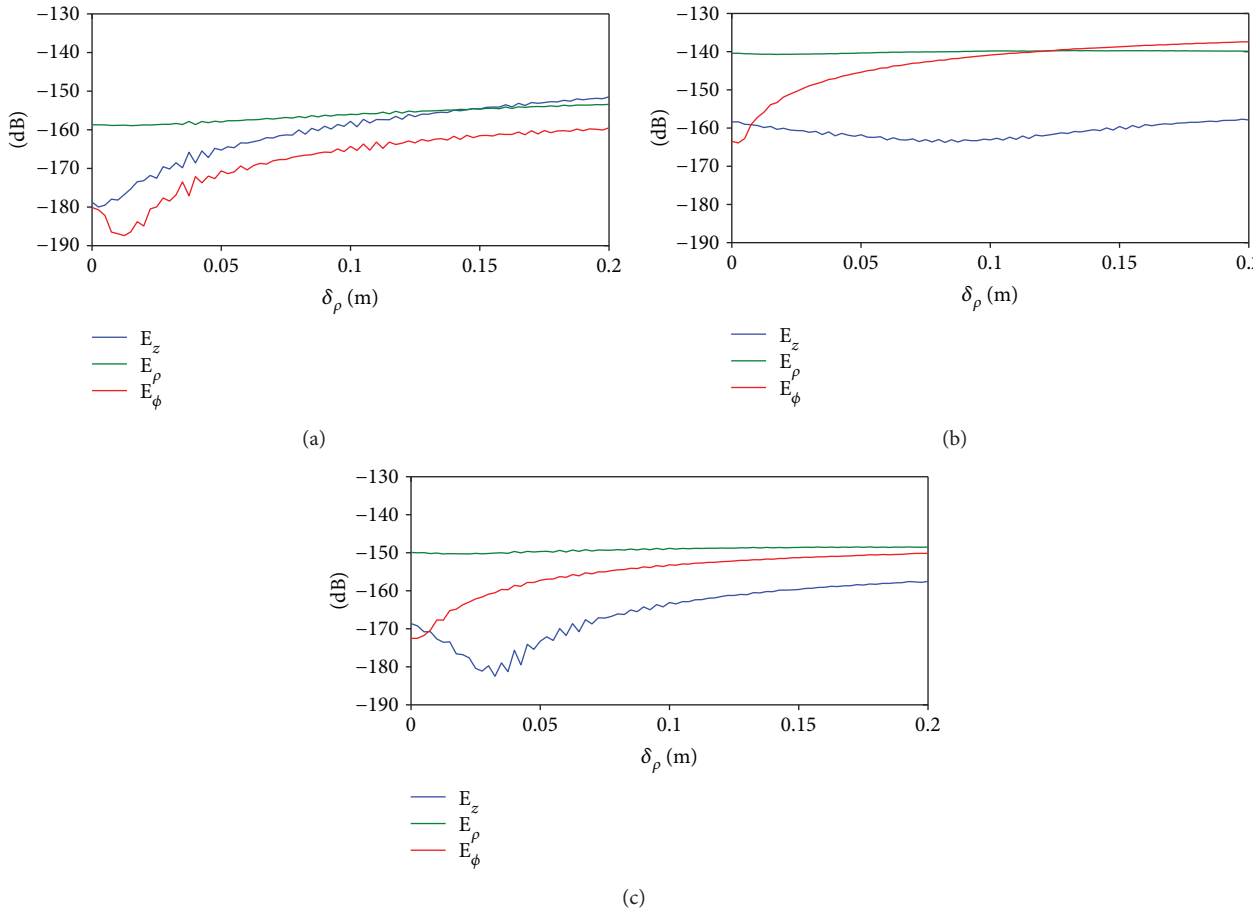

Figure 9: Field polarization distribution on horizontal circle $\delta_z = 0.4$ m and $\delta_\phi = \pi/2$. (a) Source in polarization z. (b) Source in polarization ρ. (c) Source in polarization ϕ.

$\delta_z = 0.4$ m, $\delta_\phi = \pi/2$, as a reference location in the linear decaying region, is shown in Figure 9. It shows that the strength of E_ρ remains dominant in the region $\delta_\rho \in [0\ 0.1]$, regardless of the source polarization directions. When δ_ρ increases, all the polarization components receive quasi-linear increase as a consequence of the weakening of the body scattering effect in Figure 9(a). The increasing of δ_ρ of the circles will lead to a quick convergence of the strength levels of E_ϕ towards E_ρ, while E_ρ remains a constant distribution at different δ_ρ in Figures 9(b) and 9(c).

These indicate that the field of the receiver in polarization ρ is almost free from the body scattering effect and the receiving antenna can generally obtain the decent component of the field, which is also the proof of V-polarization convergence. In order to more directly reflect the similarities and differences between measurement and simulation, the field source in the three polarization directions, the main polarization characteristics of on-body channels, and the receiver are summarized in Table 6.

Table 6: The comparative polarization characteristic.

Conditions	Measurement	FDTD simulation
Source in polarization Z/z	Cross-polarization	Cross-polarization
Source in polarization V/ρ	Copolarization	Copolarization
Source in polarization H/ϕ	Strong depolarization	Cross-polarization
The receiver	V-convergence	ρ-Convergence

5. Conclusions

In this paper, measurement results of narrowband-polarized static on-body channels at 2.4 GHz are presented under complete polarization combination in space. Analyses of the measurements demonstrate that V-polarization of the receiving antenna can effectively reduce the path loss and capture signal waves. When the transmitting antenna of the on-body channels adopts V-polarization, depolarization of on-body channels is more serious in the sitting posture due to the effect of leg scattering. The receiving antenna with V-polarization is more beneficial to obtain the decent field component compared with the Z- and H-polarizations of the receiver by analyzing the depolarization characteristics of static on-body channels, regardless of the polarization direction of the transmission antenna. This once again proved that

the receiving antenna with V-polarization can effectively reduce the path loss. The FDTD simulation results demonstrate the advantage of receiving field strength in polarization direction ρ compared with other polarization components and further validating the conclusions of our measurement analysis. The results of both simulation and measurement show that on-body propagation channels with the transmitter-adopted V- or Z-polarization generally have good polarization characteristics. Depolarization is easy to occur when the transmitter adopted H-polarization, which is different from the simulation results due to the actual complexity of the human body.

Data Availability

All measurement data in this paper has been listed in the article content, which is available to all peers and can be used in related research.

Conflicts of Interest

The authors declare that there is no conflict of interest regarding the publication of this paper.

Acknowledgments

Thanks are due to the communication laboratory of Nanchang University for the technical support. The work presented in this paper is supported by the Natural Science Foundation of China (NSFC) under grant no. 81460275.

References

[1] J. Bae and H. J. Yoo, "The effects of electrode configuration on body channel communication based on analysis of vertical and horizontal electric dipoles," *IEEE Transactions on Microwave Theory and Techniques*, vol. 63, no. 4, pp. 1409–1420, 2015.

[2] X. Lu, X. Chen, G. Sun, D. Jin, N. Ge, and L. Zeng, "UWB-based wireless body area networks channel modeling and performance evaluation," in *2011 7th International Wireless Communications and Mobile Computing Conference*, pp. 1929–1934, Istanbul, Turkey, 2011, IEEE.

[3] Q. H. Abbasi, M. U. Rehman, H. T. Chattha et al., "Ultra wideband antenna diversity characterisation for off-body communications in an indoor environment," *IET Microwaves, Antennas & Propagation*, vol. 8, no. 14, pp. 1161–1169, 2014.

[4] J. Bae, H. Cho, K. Song, H. Lee, and H. J. Yoo, "The signal transmission mechanism on the surface of human body for body channel communication," *IEEE Transactions on Microwave Theory and Techniques*, vol. 60, no. 3, pp. 582–593, 2012.

[5] Y. Li, D. Xue, E. Forrister, G. Lee, B. Garner, and Y. Kim, "Human activity classification based on dynamic time warping of an on-body creeping wave signal," *IEEE Transactions on Antennas and Propagation*, vol. 64, no. 11, pp. 4901–4905, 2016.

[6] V. Pleskachev, I. Vendik, O. Vendik, V. Kirillov, P. Turalchuk, and M. Odit, "On-body surface electromagnetic wave propagation: modeling and measurements," in *2016 10th European Conference on Antennas and Propagation (EuCAP)*, pp. 1–5, Davos, Switzerland, 2016, IEEE.

[7] T. Aoyagi, M. Kim, J.-I. Takada, K. Hamaguchi, and R. Kohno, "Numerical simulations for dynamic WBAN propagation channel during various human movements," in *2011 5th International Symposium on Medical Information and Communication Technology*, pp. 65–69, Montreux, Switzerland, 2011, IEEE.

[8] K. Li, K. Honda, and K. Ogawa, "On-body polarization-controlled active antenna to enhance signal power in human dynamic channels," in *2014 International Symposium on Antennas and Propagation Conference Proceedings*, pp. 93-94, Kaohsiung, Taiwan, 2014, IEEE.

[9] K. Li, K. Honda, and K. Ogawa, "Analysis of the body proximity cross-polarization power ratio in a human walking motion," in *2015 Asia-Pacific Microwave Conference (APMC)*, pp. 1–3, Nanjing, China, 2015, IEEE.

[10] L. Petrillo, T. Mavridis, J. Sarrazin, A. Benlarbi-Delai, and P. De Doncker, "Statistical on-body measurement results at 60 GHz," *IEEE Transactions on Antennas and Propagation*, vol. 63, no. 1, pp. 400–403, 2015.

[11] Y. I. Nechayev, C. C. Constantinou, X. Wu, and P. S. Hall, "De-polarization of on-body channels and polarization diversity at 60 GHz," *IEEE Transactions on Antennas and Propagation*, vol. 62, no. 12, pp. 6519–6523, 2014.

[12] Y. Zhao, Y. Hao, A. Alomainy, and C. Parini, "UWB on-body radio channel modeling using ray theory and subband FDTD method," *IEEE Transactions on Microwave Theory and Techniques*, vol. 54, no. 4, pp. 1827–1835, 2006.

[13] P. S. Hall and Y. Hao, "Antennas and propagation for body centric communications," in *2006 First European Conference on Antennas and Propagation*, pp. 1–7, Nice, France, 2006, IEEE.